Journal of Materials Chemistry A

ROYAL SOCIETY OF CHEMISTRY

PAPER

View Article Online
View Journal | View Issue

Check for updates

Cite this: J. Mater. Chem. A, 2025, 13, 22039

Anti-clogging and anti-tangling fog harvesting with 3D-printed mesh-harp hybrids†

Jimmy K. Kaindu,‡[a] Lilly E. Olejnicki,‡[b] Brook S. Kennedy[b] and Jonathan B. Boreyko *[a]

Received 4th April 2025
Accepted 29th May 2025

DOI: 10.1039/d5ta02686e

rsc.li/materials-a

Fog harvesting is a promising method for freshwater collection in arid regions, but existing designs are inefficient. Mesh harvesters clog easily, diverting the fog stream, while fog harps suffer from elastocapillary wire tangling, creating large gaps for diminished performance. To practically bypass both the clogging and tangling issues, we develop 3D-printed mesh-harp hybrids that increase the fog harvesting efficiency by a factor of 2–8 compared to a pure mesh or fog harp. The optimal spacing of dilute cross-support features to enable anti-tangling for an untensioned mesh-harp hybrid is rationalized by an elastocapillary model.

1 Introduction

At least a third of the world's population is combating water scarcity.[1] One promising approach to mitigate water shortages in arid regions is to harvest microscopic fog droplets by intercepting them from their streamlines.[2,3] Large-scale fog harvesting structures can collect thousands of liters of water per day when deployed in sufficient numbers.[4–9] For example, large-scale Raschel mesh nets, spanning 5000 m^2, successfully collected an annually-averaged 15 000 L per day.[10]

Although mesh-based harvesters are lightweight and easy to install, they suffer from a very low fog harvesting efficiency due to their dual constraint problem.[6,11–13] Meshes with larger holes (*ex.*: Raschel mesh) fail to intercept most of the microdroplets, but meshes with smaller holes (*ex.*: square weave) suffer from clogging.[13] The latter clogging issue is due to aggressive droplet pinning on the horizontally-oriented wires, causing the fog stream to flow around the harvester (Fig. 1a). Applying non-wetting coatings to a mesh can partially reduce the clogging issue but have cost, durability, and contamination concerns.[13–15] Even when avoiding both extremes of the dual constraint by selecting intermediate hole sizes, mesh harvesters exhibit very low fog collection efficiencies of $\eta \approx 2$–6% in lab tests,[7,13,16] where η is the ratio of harvested water to the total present in the fog stream.

Inspired by California redwoods, fog harps were developed to bypass the clogging issue inherent to mesh harvesters.[16] Redwoods collect approximately 35% of their annual water intake from fog dripping from parallel arrays of needle-like leaves.[11] Fog harps mimic redwood needles by fixing a vertical wire array within a supporting frame.[6,16–20] For both the redwood needles and the fog harp, the lack of orthogonal features prevents appreciable droplet pinning. This enables ultra-effective drainage of ~0.1 μL droplets for anti-clogging functionality, even when the features are close-packed to intercept as many droplets as possible.[7,8] The result is a superior fog harvesting efficiency of $\eta \approx$ 16–17% under equivalent lab conditions.[7,21]

However, when fog harps are scaled to the standard unit harvester size of 1 m × 1 m, they are prone to substantial elastocapillary wire tangling under foggy conditions (Fig. 1c). Elastocapillary tangling is caused by droplets on adjacent wires coalescing and pulling the wires together by surface tension. The large gaps that form allow most fog droplets to pass through, reducing their collection efficiency by as much as a factor of three.[6,21] The extent of tangling is governed by a balance between surface tension and the bending energy of the wires, the latter of which depends on both wire geometry and how much pre-tension is applied by the frame. Recently, anti-tangling and mass-manufacturable fog harps were developed that were nearly as large (0.6 m × 0.6 m) as the standard unit size.[21] However, this required imposing an ultra-high wire tension within a reinforced frame, which is likely too heavy and expensive for most practical real-world applications.

Here, we develop hybrid mesh-harp (MH) fog harvesters that simultaneously exhibit anti-clogging and anti-tangling functionalities (Fig. 1b). These hybrids were fabricated by 3D-printing fog harps that additionally feature intermittent horizontal interconnects, to combat tangling (without resorting to tensioning). By widely varying the spacing between interconnects for different harvesters, lab tests identified the optimal hybrid design. We demonstrate that, by avoiding both clogging and tangling, hybrid MH harvesters can increase the fog

[a]Department of Mechanical Engineering, Virginia Tech, Blacksburg, VA 24061, USA. E-mail: boreyko@vt.edu

[b]School of Design, Virginia Tech, Blacksburg, VA 24061, USA

† Electronic supplementary information (ESI) available. See DOI: https://doi.org/10.1039/d5ta02686e

‡ These authors contributed equally to this work.

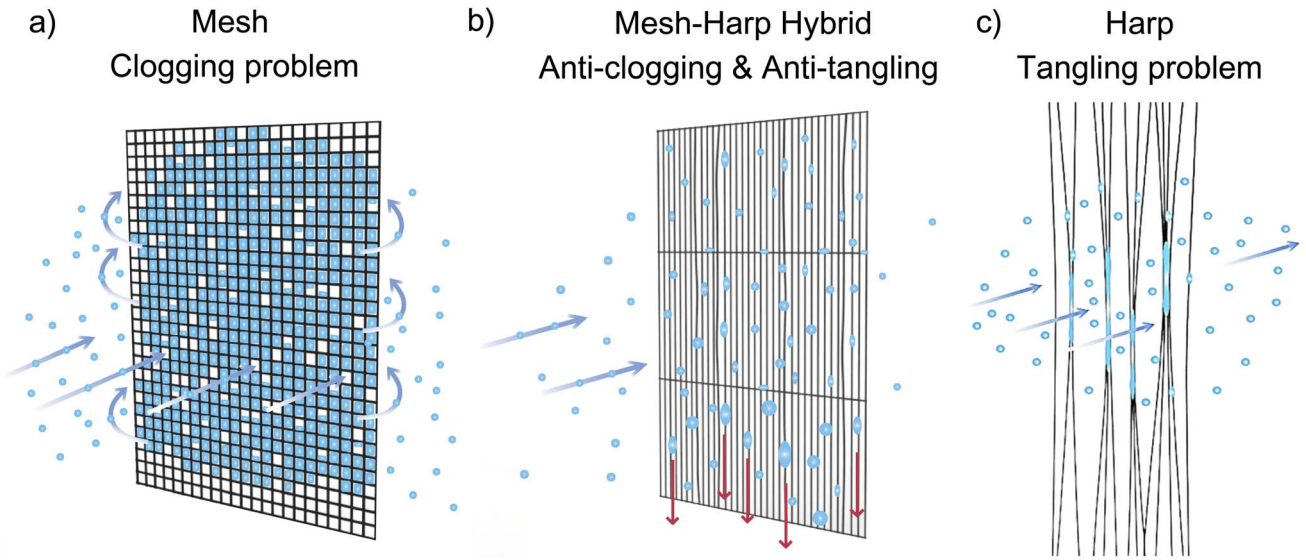

Fig. 1 Visual overview of how the performance of fog harvesters is impacted by the density of horizontal supports. (a) A conventional mesh net, featuring as many horizontal fibers as vertical ones, suffers from extensive clogging that redirects the foggy wind flow. (b) Here, we introduce a mesh-harp hybrid, comprised of close-packed vertical fibers supported by sparse horizontal inter-connects. It is designed to avoid the issues that occur on either extreme of the spectrum. (c) A fog harp is solely comprised of vertical fibers, making it prone to tangling when adjacent fog droplets coalesce together. This bundling effect opens up large holes for the fog stream to escape through.

harvesting efficiency by a factor of 2–8 compared to meshes or untensioned fog harps. Finally, a refined elastocapillary tangling model is developed to rationalize the optimal design geometry of untensioned hybrid MH harvesters for ultra-practical water harvesting.

2 Experimental section

2.1 Fabrication of mesh-harp hybrid harvesters

All fog harvesters were manufactured using 3D-printing technology (Creality, Ender-3) using polylactic acid (PLA) filaments (Hatchbox, 3D PLA-1KG1.75-BLK). PLA is composed of long chains of nonpolar lactic acid molecules, resulting in the features being weakly hydrophobic. Fig. 2 depicts the seven different scale-model fog harvesters that were 3D-printed, all of which were comprised of $d \approx 0.40$ mm diameter wires embedded within a square cross-section frame that was 308.5 mm tall and 54.5 mm wide. The two control cases were a harvester comprised of uniformly distributed vertical and horizontal wires with square-shaped holes (mesh) and one with only a vertical wire array (harp). The five hybrid harvesters are denoted by the number of horizontal interconnects that were evenly distributed along the vertical wire array (MH-131, MH-10, MH-5, MH-3, MH-1). Note that the MH-131 has exactly half the number of horizontal interconnects as the control mesh, such that the pitch between horizontal wires is twice that of the pitch between vertical wires. While the CAD designs featured wires of circular cross-section, in reality the printed wires were oval-like in cross-section due to the material expanding, with an aspect ratio of 3 : 2 (width : height). The CAD model consistently used a center-to-center pitch to wire diameter ratio (p/d) of 3.5 for the vertical wires. However, in reality, this produced wires with an actual ratio of approximately $p/d \approx 2$.

2.2 Experimental setup

Two ultrasonic humidifiers (Pure Guardian, H940AR) were distributed vertically along the center-line of a given fog harvester. The population of microscopic water droplets generated from an ultrasonic humidifier are analogous to those found in natural fog (see Fig. S1 in the ESI†). Two intensity settings were alternately used, arbitrarily termed 'moderate fog' and 'heavy fog' for this report. Using mass balances, the respective mass flow rates of the water droplet populations were measured as 1.26 g min^{-1} (top humidifier) and 1.17 g min^{-1} (bottom) for the moderate fog setting and 4.52 g min^{-1} (top) and 3.96 g min^{-1} (bottom) for the heavy fog setting. Using a cloud particle spectrometer (Droplet Measurement Technologies, FM-120), the liquid water content was calculated to be 0.18 g m^{-3} for the moderate fog and 1.713 g m^{-3} for the heavy fog. 80% of the droplets were between 6–20 μm for the moderate fog setting and 7–35 μm for the heavy setting.

Each humidifier was equipped with vinyl tubing, 2.5 cm inner diameter, to direct the fog streams horizontally toward the harvester. The centers of the tubes were vertically positioned 50.8 mm and 152.4 mm from the top frame of the harvester, respectively, and each tube outlet was 50.8 mm from the front face of the harvester. A collection container was placed beneath the fog harvester being tested. Experiments were conducted in intervals of five trials for each harvester type and fog setting, with each trial spanning 10 min. To ensure steady-state harvesting conditions, all trials were initiated only after a minimum of 30 min of continuous fog streams impacting the harvester.

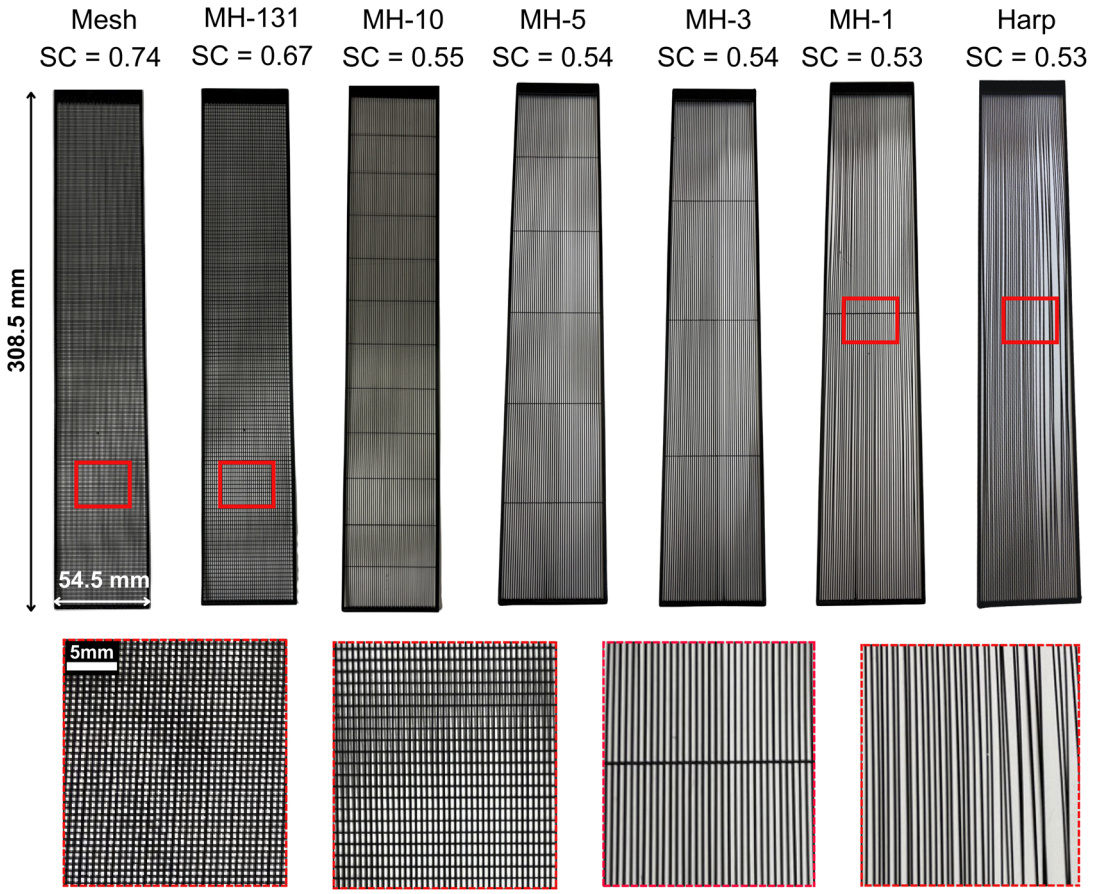

Fig. 2 Photographs of the seven 3D-printed fog harvesters characterized here, with overlying labels and measured shade coefficients (SC). The shade coefficient is defined as a ratio of projected areas: the solid features (measured using ImageJ) normalized by the overall size of the harvester. Insets are zoomed-in to better visualize individual features for the mesh, MH-131, MH-1, and harp.

3 Results and discussion

3.1 Fog harvesting efficiency

Fig. 3 shows the average fog harvesting efficiency of the various harvesters, for both moderate and heavy fog conditions. For the moderate fog setting, the mesh exhibited the lowest efficiency ($\eta_{\text{Mesh}} \approx 0.67\%$), the harp's performance was better but still quite poor ($\eta_{\text{Harp}} \approx 1.5\%$), while the MH-5 hybrid exhibited the highest efficiency ($\eta_{\text{MH-5}} \approx 5.7\%$). Put another way: the fog harp was three times more effective than the mesh by avoiding the clogging issue, but the hybrid was ten times better than the mesh by avoiding both clogging and tangling. Switching to a heavy fog, the harp was now the worst-performing due to extreme elastocapillary wire tangling ($\eta_{\text{Harp}} \approx 4.8\%$) being even more problematic than the clogging issue of the mesh ($\eta_{\text{Mesh}} \approx 6.0\%$). The MH-3 hybrid exhibited the highest collection efficiency ($\eta_{\text{MH-3}} \approx 12.7\%$), but the MH-5 was nearly as effective ($\eta_{\text{MH-3}} \approx 12.5\%$), making it the best all-around performer across multiple fog settings. In general, non-monotonic bell curves were obtained when plotting η against the harvester types, showing that hybrids are generally superior to both pure meshes and pure (untensioned) fog harps.

The fog harvesting efficiencies shown in Fig. 3 are non-dimensional ratios; Fig. S2† replots the same curves to quantify in terms of the water harvesting mass flux. For the moderate fog setting, the MH-5 exhibited the highest mass flux of $J_{\text{MH-5}} \approx 1.18\ \text{kg m}^{-2}\ \text{h}^{-1}$. For the heavy fog setting, the MH-3 exhibited the highest mass flux of $J_{\text{MH-3}} \approx 9.26\ \text{kg m}^{-2}\ \text{h}^{-1}$.

Fig. 4 shows corresponding images during fog harvesting on each harvester type. The pictures confirm the hypothesis that the mesh (and MH-131) exhibit extensive clogging, while the harp (and MH-1) are plagued by heavy tangling. The best-performing hybrid from Fig. 3, MH-5, was visually confirmed to minimize both clogging and tangling. Photographs reveal that MH-3 still exhibits minor tangling. This explains why η for MH-3 is slightly less than MH-5 for the moderate fog setting, where η is known to be especially sensitive to the tangling problem.[7] Images also highlight that the greater the number of interconnects, the more large droplets are pinned to the harvester. This in turn rationalizes why MH-3 is the best-performing for the heavy fog setting despite the minor tangling, because the greater number of pinned droplets on MH-5 and especially MH-10 (analogous to minor "clogging") outweighs the benefit of avoiding minor tangling.

3.2 Clogging and tangling histograms

Fig. 5a shows a histogram to quantify how the extent of clogging varies with the harvester type. To evaluate clogging percentages,

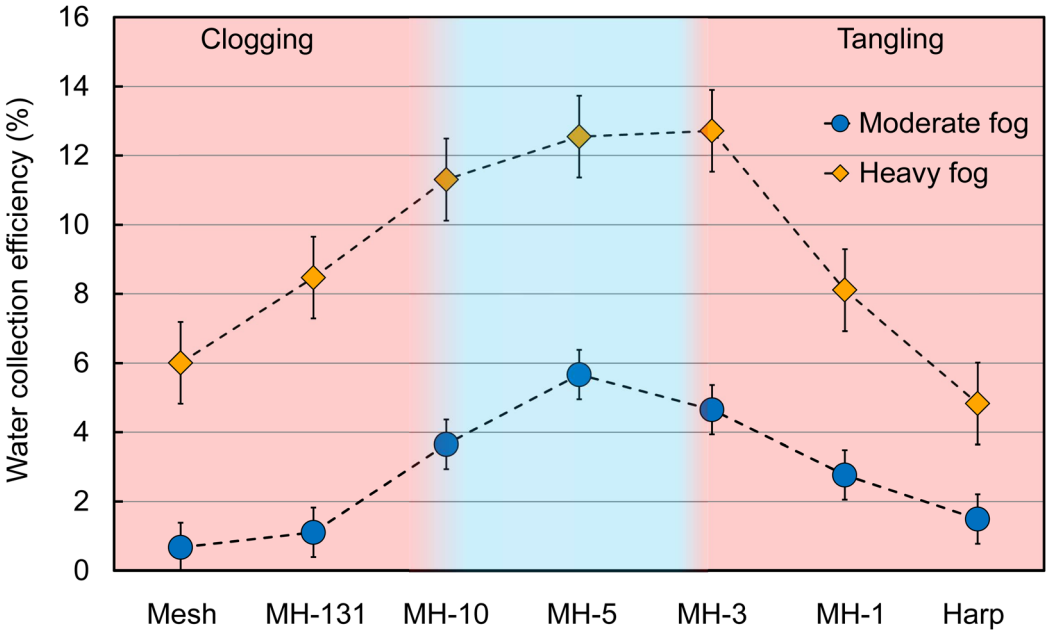

Fig. 3 Collection efficiency of each harvester type under moderate and heavy fog conditions. The red regimes indicate the undesirable extremes of clogging (left band) and tangling (right band), while the blue regime denotes hybrid harvesters exhibiting anti-clogging and anti-tangling functionalities. Total mass flow rates from both humidifiers were 2.43 g min^{-1} for moderate fog (diamonds) and 8.48 g min^{-1} for heavy fog (circles). Error bars represent a standard deviation from the average of five trials.

10 rows were randomly selected from the central region of the fog harvester, ensuring accurate representation by avoiding the first row adjacent to each frame edge, where boundary effects may influence droplet accumulation. The clogging percentage for each wire was calculated by assessing the proportion of wire surface area covered by coalesced droplets relative to the total wire surface area. For the heavy fog setting, over 80% of the holes were fully clogged for the mesh. In contrast, only about 25% of the holes of the half-mesh (MH-131) were fully clogged, although another 25% exhibited partial clogging. This further validates the performance results from Fig. 3, where the MH-131 always outperformed the mesh. The other harvesters did

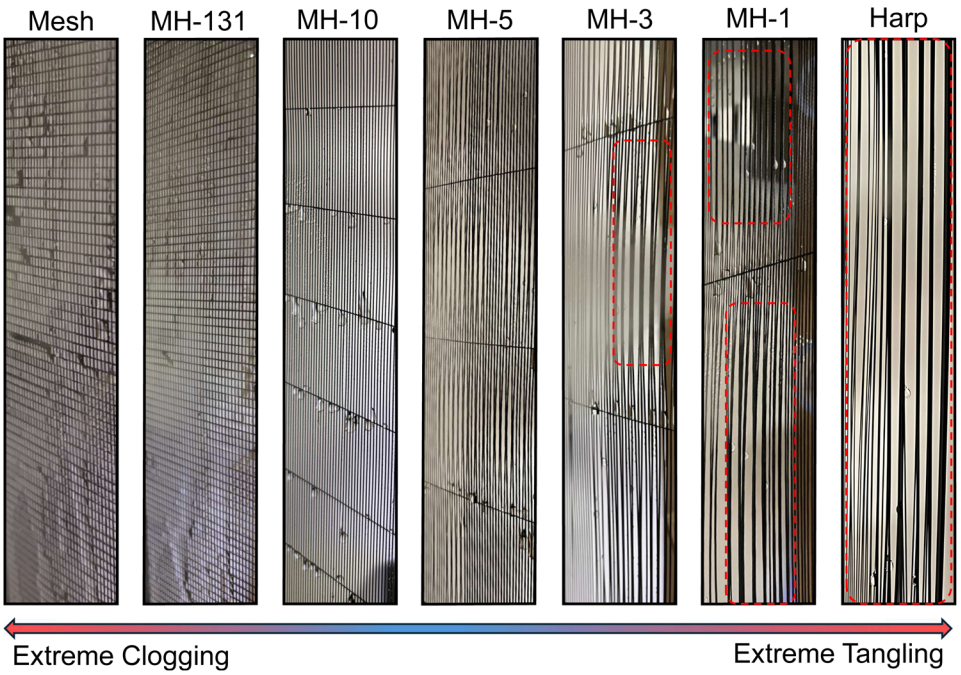

Fig. 4 Photographs of all harvesters during fog harvesting, with red dotted regions highlighting elastocapillary tangling. See Movies S1–S3 in the ESI† for fog droplets collecting on the mesh, MH-10, and harp harvesters, respectively.

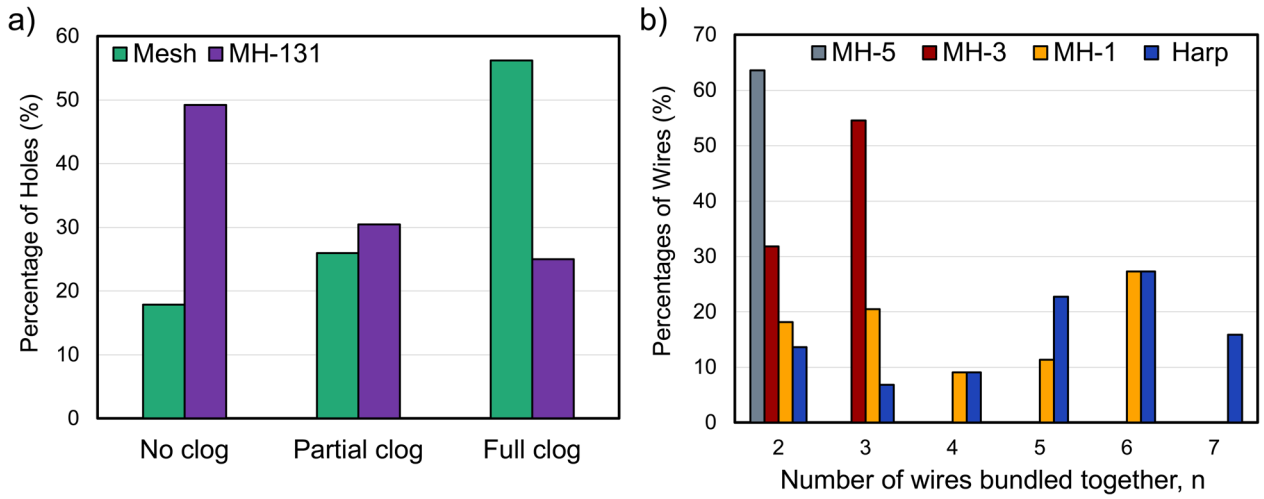

Fig. 5 (a) Histogram quantifying the extent of clogging for the mesh and MH-131. Holes that remain completely open are binned into the 'No clogging' category, holes at least partially blocked with a water film are 'partial clogging,' and holes completely closed with water are 'full clogging.' (b) Histogram quantifying the extent of elastocapillary wire tangling for the MH-5, MH-3, MH-1, and harp harvesters. Note that $n = 1$ (*i.e.*, non-tangled single wires) are omitted, such that the total percentage for a given harvester corresponds to the fraction of wires that are tangled to any extent.

not demonstrate appreciable clogging, aside from the aforementioned secondary issue of pinned droplets along the interconnects.

Fig. 5b quantifies the elastocapillary tangling issue. The pure harp exhibited up to seven-wire bundles, highlighting the severity of the tangling problem in the absence of impractical tensioning. With more interconnects, this issue gradually improves: the worst-case scenario improves to six-wire bundles for MH-1, three-wire bundles for MH-3, and only two-wire bundles for MH-5. The fact that MH-5 exhibits the highest possible η suggests that two-wire tangling states do not open up large-enough holes in the harvester to compromise the deposition efficiency of droplets. Previous reports have also shown that droplets can slide very effectively between two adjacent wires.[16] Indeed, even the very minor increase of pinned droplets on the MH-10 is clearly a net detriment to η despite the complete lack of even two-wire tangling states. Therefore, it seems that tangling is only a problem for three-wire bundles and beyond.

3.3 Elastocapillary tangling model

Here, we develop an elastocapillary tangling model that improves on those developed in previous reports. Py *et al.* and Duprat *et al.* modeled the critical length of two parallel, cantilevered wires where capillarity overcomes the elastic energy required to bend them together.[22,23] Shi *et al.* contextualized this model for fog harps by assuming the wires were pinned at both ends (effectively doubling the critical length) and allowing for a pre-tension in the wires to modify the overall bending energy.[6] The existing theory on elastocapillary tangling in tensioned fog harps can be summarized by the following equation:[7]

$$2\gamma(\pi - 2)R_{\text{wire}}L_{\text{dry},n}{}^4 - (TL_{\text{dry},n}{}^2 + 9EI)[(n-1)^2(p/2 - R_{\text{wire}})^2] = 0 \quad (1)$$

where γ represents the surface tension of water, R_{wire} is the radius of each wire, and $L_{\text{dry},n}$ denotes the minimum vertical length required for n wires to bundle together from either end of the frame, T is the applied pretension in the wires, p is the center-to-center pitch between wires, E is the Young's modulus, and I is the area moment of inertia for a wire (assuming a circular cross section).

This previous model had the harp wires under pre-tension to prevent tangling. In contrast, the 3D-printed harvesters fabricated here do not exhibit appreciable pre-tension. In the absence of pre-tension, we can no longer neglect the axial tension resulting from the elongation of the wires as they bend. Further, the original model assumed a simply supported beam (pinned–pinned), where both ends are supported but free to rotate. This assumption was reasonable for the context of threading a wire along a series of holes[16] or comb teeth,[6,7] but not for the present case of 3D-printed fibers held within a continuous frame. We therefore change the model here to give the fibers a fixed–fixed (clamped–clamped) support. These updates collectively result in the following expression:

$$2\gamma(\pi - 2)R_{\text{wire}}L_{\text{dry},n}{}^4 - (T_{\text{axial}}L_{\text{dry},n}{}^2 + 24EI)[(n-1)^2(p/2 - R_{\text{wire}})^2] = 0 \quad (2)$$

where the first (unchanged) term represents the energy gained from coalescing wetted fibers together, the second term accounts for axial tension from elongation, and the third term captures the bending energy of the fibers with fixed–fixed supports. The axial tension variable due to elongation is in turn defined as:

$$T_{\text{axial}} = \frac{EA\Delta L_{\text{axial}}}{L_{\text{wire}}}, \quad (3)$$

where A is the cross-sectional area of each fiber, L_{wire} is the total length of a given vertical fiber (prior to elongation), and ΔL_{axial} is the axial elongation of the fiber due to bending. A critical fiber length, beyond which a bundle of n fibers is possible for the first

time, is expressed as $L_{wire,c} = 2L_{dry,n}$. Fiber elongation can be approximated using the Pythagorean theorem (Fig. S3†): ${L_{diagonal}}^2 = \Delta{L_{horizontal}}^2 + {L_{dry,n}}^2$, where by definition $\Delta L_{axial} = L_{diagonal} - L_{dry,n}$ and the lateral extent of the bending for the outermost fibers is given by:

$$\Delta L_{horizonal}(n,p,D) = \begin{cases} \left(\frac{n}{2}-1\right)(p-D)+\frac{p-D}{2} & \text{if } n \text{ is even} \\ \left(\frac{n-1}{2}\right)(p-D) & \text{if } n \text{ is odd} \end{cases} \quad (4)$$

Utilizing this updated model, Fig. 6a shows a phase map predicting the maximum tangling state for any given value of p and L_{dry}. A reminder that L_{dry} can be conceptualized as the critical half-length of a fiber, $L_{wire,c}/2$, beyond which bundles of n fibers becomes possible. For the harp, L_{wire} is given by the vertical span of each fiber within the overall frame, whereas for the hybrid harvesters, it represents the span between two adjacent inter-connects. The wire lengths for harvesters that exhibited tangling are as follows: harp harvester $L_{wire} \approx 300$ mm, MH-1 $L_{wire} \approx 150$ mm, MH-3 $L_{wire} \approx 77$ mm, and MH-5 harvester $L_{wire} \approx 55$ mm. No bundling should be possible beneath the $n = 2$ phase line, only two-wire bundling should be possible between the $n = 2$ and $n = 3$ phase lines, both two-wire and three-wire bundling are possible between the $n = 3$ and $n = 4$ phase lines, *etc.* Experimental data points are overlaid using the harp, MH-1, MH-3, and MH-5 harvesters where elastocapillary tangling occurred. There is excellent agreement between the maximal value of n observed for each harvester and the theoretical prediction of n.

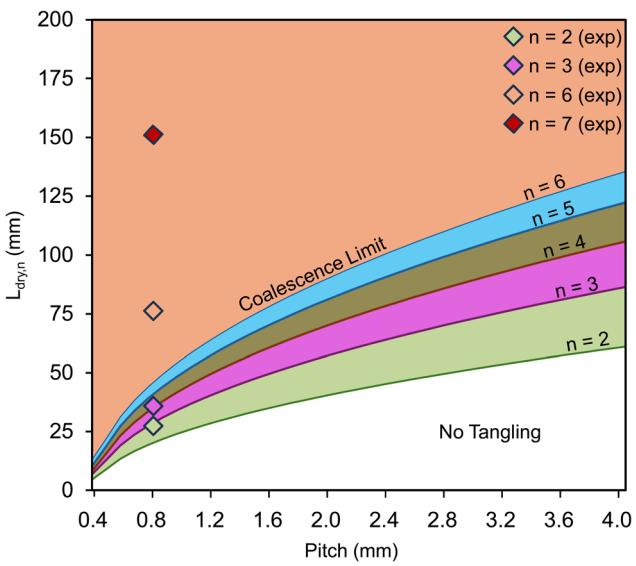

Fig. 6 Theoretical phase map predicting tangling onset as a function of wire length and pitch. Above each phase boundary, tangling is possible for two (green), three (purple), four (brown), five (blue), and six (orange) wires. Experimental data points for a 0.8 mm pitch follow the same color scheme, with the chosen value for $L_{dry,n}$ corresponding to $L_{wire}/2$.

One final nuance of this updated analytical model is accounting for an upper limit to n that we term the coalescence limit. This accounts for the practical reality that, for increasingly large bundles to stick together, adhered fog droplets must be able to span the gap between existing bundles to trigger further coalescence and bundling. The critical droplet size, beyond which sliding occurs, can be estimated by balancing the gravitational and pinning forces. Kawasaki, Furmidge, and others demonstrated that the pinning force arises from contact angle hysteresis and is dominant along the receding contact line.[24,25] Shi *et al.* applied this model to calculate the theoretical critical volume for a droplet to slide down a harp wire.[16] Here, we develop the coalescence limit using the simplest possible scenario of two hemi-spherical and same-sized droplets that are facing each other as they grow from two neighboring and same-sized bundles (Fig. S4†). Assuming the receding contact line of either droplet wets a half-perimeter of an outer-most fiber within its bundle, the pinning force is estimated by $F_{pinning} \approx \pi R_{wire}\gamma(\cos\ \theta_r - \cos\ \theta_a)$, where $\cos\ \theta_r \approx 50° \pm 2°$ and $\cos\ \theta_a \approx 120° \pm 4°$ are the advancing and receding apparent contact angles, respectively, on the PLA fibers. See Movie S4† for a sample trial of a droplet sliding down a PLA fiber to measure θ_r and θ_a, where the uncertainty reported above represents one standard deviation across three trials. For approximately hemispherical droplets the gravitational force is $F_g \approx (2\pi/3)R^3\rho g$, where R is the droplet radius. Coalescence and further bundling should occur at $R_{coalesce} \approx \Delta L_{horizontal} + ((p-D)/2)$, where the n used to calculate $\Delta L_{horizontal}$ corresponds to that of either sub-bundle. Finally, the coalescence limit is found for the smallest value of n where $R_{coalesce} > R_c$:

$$\Delta L_{horizontal} + \frac{p-D}{2} > \left(\frac{3R_{wire}\gamma(\cos\theta_r - \cos\theta_a)}{4\rho_{water}g}\right)^{1/3}, \quad (5)$$

where n is twice that used to calculate $L_{horizontal}$ each sub-bundle. Beyond the coalescence limit, droplet sliding always occurs before the sub-bundles can merge together.

Fig. 7 calculates the coalescence limit for our case of $p \approx 0.80$ mm, $D \approx 0.40$ mm, $\cos\theta_r \approx 50°$, and $\cos\theta_a \approx 120°$. For simplicity, we only found $R_{coalesce}/R_c$ for even values of n, in keeping with our simplifying assumption of same-sized sub-bundles (*i.e.*, $n/2$) and $\Delta L_{horizontal}$ values. The critical value of $R_{coalesce}/R_c \approx 1$ was reached at $n = 6$. This suggests that adjacent fog droplets can barely manage to coalesce before sliding when they are on opposing three-fiber sub-bundles, but that no coalescence should be possible for four-fiber sub-bundles or larger. Using imaging to verify: a characteristic gap between two neighboring four-wire bundles was about 4 mm, while even the largest adhered fog droplets exhibited had a radius of $R \approx 2.0$ mm (Fig. S4†). This is in good agreement with our experimental observations of the harp, where $n = 6$ had multiple occurrences but never $n = 8$ or greater (Fig. 5b). There was a single instance of $n = 7$ for the harp, which we attribute to sliding droplets accumulating multiple daughter droplets to enable a rare coalescence event that extends just beyond the quasi-static coalescence limit. For the hybrid harvesters, note that the much shorter values of L_{wire} resulted in the bending

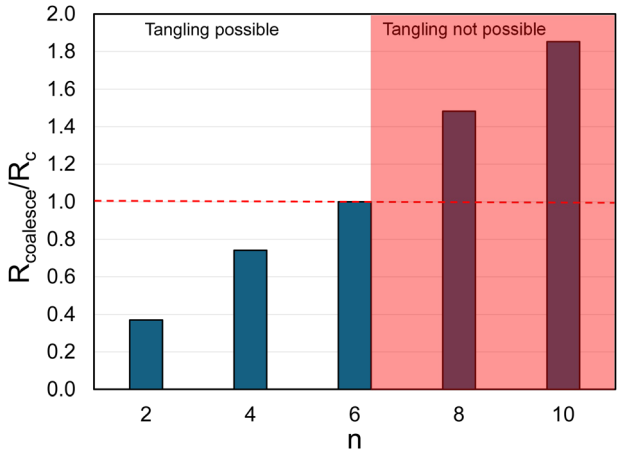

Fig. 7 The histogram displays the ratio $R_{coalescence}/R_c$ (droplet radius to the radius required for coalescence) against the number of fibers in a bundle, illustrating the transition between successful coalescence ($R_{coalescence}/R_c < 1$) and failure ($R_{coalescence}/R_c > 1$). The coalescence limit was reached at $n = 6$, beyond which droplets slide before merging. This model assumes only even-numbered bundle pairings (*e.g.*, 1 + 1, 2 + 2, 4 + 4), simplifying real-world bundling behavior by neglecting asymmetric interactions. Experimentally, coalescence was observed up to $n = 6$ but not at $n = 8$, supporting analytical predictions.

limit (*i.e.*, eqn (2)) superseding the coalescence limit to prescribe the maximal n value, such that the latter was only testable for the pure harp.

As an alternative to the analytical tangling model, it may be desirable to utilize a recursive tangling model especially for larger n values. This is because for $n > 2$, only the bending energy of the outermost wires was considered for the analytical model, as they experience the greatest displacement. However, the cumulative bending energy of all wires becomes more appreciable as n increases. Additionally, the analytical model only accounted for the surface energy change of wetted fibers coming together on either end of a bundle, but this would ignore coalescence events occurring in the middle for $n \geq 4$. These limitations were solved by Kaindu *et al.* by developing a recursive tangling model that incorporated the cumulative effects of bending and surface energy for any value of n for tensioned harp wires.[21] Here, we adapted the recursive model to the present context of zero pre-tension, axial tension *via* fiber elongation, and fixed–fixed fiber support. Interestingly, numerical solutions of this updated recursive modeled over-predicted the maximal extent of tangling more so than the simpler analytical model, such that the latter is both more accurate and easier to solve. For this reason, the full derivation and graphical representation of the recursive model is not shown here but can be seen in full in the ESI (Fig. S5).†

The long-term sustainability of PLA in 3D-printed coatings or fibers warrants consideration, given that PLA is known to degrade under natural outdoor conditions.[26] This raises concerns about the long-term harvester durability and environmental impact of using PLA in large-scale fog harvesting systems. However, the core innovation of this work lies not in the material choice, but in the design functionality: we demonstrate that introducing intermittent cross-supports is an effective, scalable solution to the wire tangling problem—one that does not depend on fiber tensioning. For commercial implementation, the cross-support design could be fabricated using alternative approaches such as metal 3D printing or more sustainable plastics like polyhydroxyalkanoates (PHAs)[27] and polybutylene succinate (PBS).[28] Moreover, non-additive manufacturing routes are also viable. Industrial-scale production might exploit roll-to-roll stamping,[29] adapt existing harp screen processes,[21] or even reprogram textile looms to incorporate the support geometry.[30] Regardless of the chosen manufacturing method, the design principle we establish—intermittent horizontal interconnects to suppress tangling—remains the key contribution and can be adapted to diverse materials and production strategies.

4 Conclusion

We have demonstrated that 3D-printed mesh-harp (MH) hybrid fog harvesters effectively combine the anti-clogging functionality of fog harps with the anti-tangling functionality of mesh nets, overcoming the limitations of both traditional systems. Hybrid fog harvesters increased the water collection efficiency by as much as a factor of 8.5 compared to equivalent mesh nets and 3.8 compared to equivalent fog harps. We developed an improved model for predicting the extent of wire tangling that accounted for bending-induced axial tension to more accurately quantify the competition between elasticity and capillarity. We also revealed a coalescence limit, beyond which, droplet coalescence and fiber bundling are impossible even when hypothetically favored by elastocapillary considerations alone. These findings show that hybrid harvesters can effectively collect water without suffering from clogging (unlike nets) or requiring an impractical pre-tension to avoid tangling (unlike harps).

Data availability

The data supporting this article have been included as part of the ESI.†

Conflicts of interest

The authors declare that they have no known competing financial interests or personal relationships that could have appeared to influence the work reported in this paper.

Acknowledgements

This work was supported by Comstock Innovations Corporation. We thank Nicholas G. Kowalski for fruitful discussions on the elastocapillary tangling model.

References

1 A. E. Ercin and A. Y. Hoekstra, Water footprint scenarios for 2050: A global analysis, *Environ. Int.*, 2014, **64**, 71–82.

2 Y. Jiang, C. Machado and K. C. K. Park, From capture to transport: A review of engineered surfaces for fog collection, *Droplet*, 2023, **2**, e55.
3 B. S. Kennedy and J. B. Boreyko, Bio-inspired fog harvesting meshes: A review, *Adv. Funct. Mater.*, 2024, **34**, 2306162.
4 O. Klemm, R. S. Schemenauer, A. Lummerich, P. Cereceda, V. Marzol, D. Corell, J. van Heerden, D. Reinhard, T. Gherezghiher, J. Olivier, P. Osses, J. Sarsour, E. Frost, M. J. Estrela, J. A. Valiente and G. M. Fessehaye, Fog as a fresh-water resource: Overview and perspectives, *Ambio*, 2012, **41**, 221–234.
5 M. Quadir, G. Jiménez, R. Farnum, L. Dodson and V. Smakhtin, Fog water collection: Challenges beyond technology, *Water*, 2018, **10**, 372.
6 W. Shi, L. H. De Koninck, B. J. Hart, N. G. Kowalski, A. P. Fugaro, T. W. van der Sloot, R. S. Ott, B. S. Kennedy and J. B. Boreyko, Harps under heavy fog conditions: superior to meshes but prone to tangling, *ACS Appl. Mater. Interfaces*, 2020, **12**, 48124–48132.
7 N. G. Kowalski, W. Shi, B. S. Kennedy and J. B. Boreyko, Optimizing fog harps, *ACS Appl. Mater. Interfaces*, 2021, **13**, 38826–38834.
8 W. Shi, T. W. van der Sloot, B. J. Hart, B. S. Kennedy and J. B. Boreyko, Harps enable water harvesting under light fog conditions, *Adv. Sustainable Syst.*, 2020, **4**, 2000040.
9 R. S. Schemenauer and P. Cereceda, A proposed standard fog collector for use in high-elevation regions, *J. Appl. Meteorol.*, 1994, **33**, 1313–1322.
10 R. S. Schemenauer, P. Cereceda, and P. Osses, *FogQuest: Fog Water Collection Manual*, 2015.
11 H. R. Byers, Coastal redwoods and fog drip, *Ecology*, 1953, **34**, 192–193.
12 M. Cao, J. Ju, K. Li, S. Dou, K. Liu and L. Jiang, Facile and large-scale fabrication of a cactus-inspired continuous fog collector, *Adv. Funct. Mater.*, 2014, **24**, 3235–3240.
13 K. C. K. Park, S. S. Chhatre, S. Srinivasan, R. E. Cohen and G. H. McKinley, Optimal design of permeable fiber network structures for fog harvesting, *Langmuir*, 2013, **29**, 13269–13277.
14 J. D. Smith, R. Dhiman, S. Anand, E. Reza-Garduno, R. E. Cohen, G. H. McKinley and K. K. Varanasi, Droplet mobility on lubricant-impregnated surfaces, *Soft Matter*, 2013, **9**, 1772–1780.
15 B. S. Lalia, S. Anand, K. K. Varanasi and R. Haskaikeh, Fog-harvesting potential of lubricant-impregnated electrospun nanomats, *Langmuir*, 2013, **29**, 13081–13088.
16 W. Shi, M. J. Anderson, J. B. Tulkoff, B. S. Kennedy and J. B. Boreyko, Fog harvesting with harps, *ACS Appl. Mater. Interfaces*, 2018, **10**, 11979–11986.
17 S. Sharifvaghefi and H. Kazerooni, Fog harvesting: combination and comparison of different methods to maximize the collection efficiency, *SN Appl. Sci.*, 2021, **3**, 516.
18 X. Yan and Y. Jiang, Numerical evaluation of the fog collection potential of electrostatically enhanced fog collector, *Atmos. Res.*, 2021, **248**, 105251.
19 N. G. Kowalski and J. B. Boreyko, Dynamics of fog droplets on a harp wire, *Soft Matter*, 2022, **18**, 7148–7158.
20 M. Azeem, A. Guérin, T. Dumais, L. Caminos, R. E. Goldstein, A. I. Pesci, J. de Dios Rivera, M. J. Torres, J. Wiener, J. L. Campos and J. Dumais, Optimal design of multilayer fog collectors, *ACS Appl. Mater. Interfaces*, 2020, **12**, 7736–7743.
21 J. K. Kaindu, K. R. Murphy, N. G. Kowalski, A. N. Jones, M. D. Fleming, B. S. Kennedy and J. B. Boreyko, Antitangling and manufacturable fog harps for high-efficiency water harvesting, *Droplet*, 2023, **2**, e78.
22 C. Py, R. Bastien, J. Bico, B. Roman and A. Boudaoud, 3D aggregation of wet fibers, *Europhys. Lett.*, 2007, **77**, 44005.
23 C. Duprat, S. Protiere, A. Y. Beebe and H. A. Stone, Wetting of flexible fibre arrays, *Nature*, 2012, **482**, 510–513.
24 K. Kawasaki, Study of wettability of polymers by sliding of water drop, *J. Colloid Sci.*, 1960, **15**, 402–407.
25 C. G. L. Furmidge, Studies at phase interfaces. I. the sliding of liquid drops on solid surfaces and a theory for spray retention, *J. Colloid Sci.*, 1962, **17**, 309–324.
26 M. R. Hasan, I. J. Davies, A. Pramanik, M. John and W. K. Biswas, Potential of recycled PLA in 3D printing: A review, *Sustainable Manufacturing and Service Economics*, 2024, **3**, 100020.
27 G. Q. Chen and M. K. Patel, Plastics derived from biological sources: Present and future: A technical and environmental review, *Chem. Rev.*, 2012, **112**, 2082–2099.
28 N. Wierckx, T. Narancic, C. Eberlein, R. Wei, O. Drzyzga, A. Magnin, H. Ballerstedt, S. T. Kenny, E. Pollet, L. Avérous, K. E. O'Connor, W. Zimmermann, H. J. Heipieper, A. Prieto, J. Jiménez and L. M. Blank, *Plastic biodegradation: Challenges and opportunities*, Springer International Publishing, 2018.
29 K. Xu, M. Yang, Y. Zhou and L. Wang, Metal mesh electrode array fabricated by plate-to-roll nanoimprint lithography, *SN Appl. Sci.*, 2020, **2**, 161.
30 X. Tian, M. Yao, Y. Li and L. Li, Design and fabrication of mesh-like four-warp leno cotton fabric based on self-locking effect: Outstanding mechanical performance and breathability, *Cellulose*, 2025, **32**, 1979–1991.

